CFD SIMULATION OF FOULING OF PLATE HEAT EXCHANGER BY PHOSPHATE CALCIUM

***U.Ojaniemi[1], T. P. Pättikangas[1], A. Jäsberg[1], E. Puhakka[2], A. Koponen[1]**
[1] VTT Technical Research Centre of Finland Ltd, P.O. Box 1000, FI-02044 VTT, Finland
[2] University of Helsinki, Department of Chemistry, P.O. Box 55, FI-00014 UNIVERSITY OF HELSINKI, Finland

ABSTRACT

A computational Fluid Dynamics (CFD) model was developed for fouling of calcium phosphate in heat exchangers which can take into account the tendency of fluid components to precipitate and the surface properties of the materials. In the CFD model the precipitation of inversely soluble mineral due to the temperature increase in the near-surface region of the heated wall was modelled based on the saturation ratio. The precipitates form small, spherical particles that can adhere on the wall surface. The wall function model developed for adherence was modified to take into account the turbulent viscosity modelled by CFD. The model was tested against experiments made with SMUF, which is an aqueous solution simulating the mineral composition of milk. This preliminary adhesion CFD model pave the route to build a more comprehensive model for predicting the likely profile of milk deposition in heat exchangers.

INTRODUCTION

The modelling of fouling mechanisms has been an interesting topic during the years. Fouling, i.e. deposition of unwanted material on heat transfer surfaces, is associated with the increased costs of maintenance, downtime and oversizing of the process equipment. In this paper the particulate fouling of plate heat exchangers is studied. The plate heat exchangers are widely applied e.g. in dairy and other food processing industries.

At present, milk fluid fouling chemistry is qualitatively well understood [1], but the behavior of the process at ultrahigh temperature (UHT) is not yet as well known. In addition to protein fouling, deposition of calcium phosphate is taking place due to the inverse solubility relation with temperature. At relatively high temperatures (above 360 K), the main deposit component is calcium phosphate. In this study, the inorganic fouling was investigated with SMUF, which is an aqueous solution simulating the mineral composition of milk.

Changes in the mineral equilibrium of SMUF due to changes in pH, temperature or of the calcium and phosphate concentration can result in more or less precipitation of calcium phosphate. During the heating process, the precipitation of calcium phosphate may take place in the core flow as well. Salting out of the precipitates produces small particles in the fluid. Lately, several authors [3 - 7] have investigated the precipitation of calcium phosphate.

In this study, a CFD model for precipitation of calcium phosphate and the precipitates adherence on a heated wall was developed. The model for the adhesion of calcium carbonate particles from dense particulate suspension presented earlier by Ojaniemi *et al*. [2] was applied and modified to take into account the turbulent viscosity modelled by CFD. The particulate fouling process can be considered as a serial process of transport into the vicinity of the wall and adherence on the surface. Adhesion on the wall depends on several surface properties, such as roughness, surface composition and surface energy.

The numerical models for the fouling process presented in literature are most often based on mass transfer to the surface or on surface reactions. The modelling of adhesion on the surface has gained less attention, even though the fouling process is generally accepted to be affected by surface properties. For the validation of the model, the experiments done with SMUF with plate heat exchanger were applied as test cases [8].

PRECIPITATION OF CALCIUM PHOSPHATE

Simulated milk ultrafiltrate (SMUF) is an aqueous salt solution simulating the mineral composition of milk serum obtained by ultrafiltration (UF). In milk, the serum phase is in a dynamic equilibrium with insoluble salts within the casein micelle. Therefore, the serum phase is saturated with respect to calcium phosphate depending on factors like pH and temperature. In this study, simulated milk ultrafiltrate (SMUF) was applied as medium where the inorganic fouling on the surfaces of heat exchanger can take place by precipitation. The construction of the SMUF solution was modified from the chemical composition developed by Dumpler *et al.* [7] (Table 1).

Calcium phosphate is the predominant inorganic salt precipitating in dairy processes and

ISBN: 978-0-9984188-1-0; Published online www.heatexchanger-fouling.com

can appear in several forms: hydroxyapatite (HAP), brushite (dicalcium phosphate dehydrate, DCPD) or octacalcium phosphate (OCT). HAP has the lowest solubility product, and therefore it is expected to salt out of the solution before the other calcium ions [3, 5]. This study is related to the precipitation of HAP, $Ca_{10}(PO_4)_6OH_2$, from the SMUF solution:

$$Ca_{10}(PO4)_6OH_2 \leftrightarrow 10Ca^{2+} + 6PO_4^{3-} + 2OH^- \quad (1)$$

Table 1. SMUF test fluid concentrations

Chemical species	Concentration mmol/L	Chemical species	Concentration mmol/L
K^+	35.5	PO_4^{3-}	10.4
Na^+	15.1	SO_4^{2-}	1.1
Mg^{2+}	2.6	Cl^-	24.9
Ca^{2+}	5.1		

In the SMUF solution, a number of salts are present in the aqueous phase. The tendency of salt to form complex or dissociate into its components is a function of ion activities and ion strength of the solution, and it is described by equilibrium constant. Equilibrium constant K_T describes the solubility of a solid substance in a chemical equilibrium in a solution of that compound.

Ion strength I for the solution is

$$I = \frac{1}{2}\sum c_i z_i^2 \quad (2)$$

where c_i is the molar concentration of species i, and z_i is the charge number of ion i. The total ion strength of the SMUF is of the order of 0.1 M. Therefore, the activity of the ion is derived from the Davies equation

$$-\log g_i = A z_i^2 \left[\frac{\sqrt{I}}{1+\sqrt{I}} - 0.2I\right], \quad (3)$$

where $A = 0.486 + 6.07\times10^{-4}T + 6.43\times10^{-6}T^2$ is determined with temperature in Celsius [9].

For the equilibrium constant K_{T1} of the reaction (1), several values are presented in literature. The constants presented at a standard state temperature T_1=298.15 K according to McDowell *et al.* [10], K_{T1}=3.04 $\cdot10^{-59}$, and K_{T1}=1.82 $\cdot10^{-58}$ applied by Mekmene *et al.* [3] were studied.

For calculating the equilibrium constant in the elevated temperatures, Eq. (4) is applied:

$$\ln\left(\frac{K_{T_2}}{K_{T_1}}\right) = \frac{\Delta H^o}{R}\left(\frac{1}{T_1} - \frac{1}{T_2}\right), \quad (4)$$

where K_{T2} is the equilibrium constant at temperature T_2, ΔH^0 is the standard reaction enthalpy and R is the universal gas constant. The standard reaction enthalpy for the reaction (1) is calculated with the standard enthalpy $\Delta H_{HAP}{}^o$ = -13385.62kJ/mol for HAP [11]. The resulting equilibrium constant K_{T2} at elevated temperatures is presented in Fig. 1.

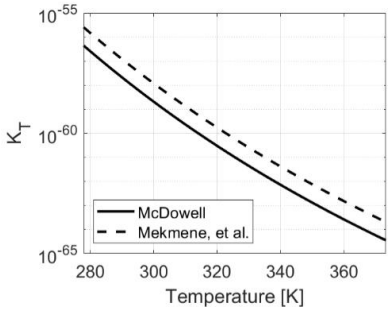

Fig. 1. Equilibrium constant K_{T2} as a function of temperature, calculated by McDowell *et al.* [10] (solid line) and by Mekmene *et al.* [3] (dashed line).

The saturation ratio is the driving force for precipitation and has been commonly applied to indication of precipitation propensity of the solution. As the saturation ratio of the solution exceeds one, precipitation is taking place. The relative saturation ratio for the reaction (1) can be calculated by equilibrium constant, K_T

$$S = \left(\frac{a(Ca^{2+})^{10}\, a(PO_4^{3-})^6\, a(OH^-)^2}{K_T}\right)^{\frac{1}{10+6+2}} \quad (5)$$

where $a(X^{Y+}) = \gamma_X c_X$, is the ion activity.

The saturation ratio in elevated temperatures for HAP is presented in Fig. 2. It has been calculated with the species concentrations applied in the experiments with the equilibrium constants by McDowell *et al.* [10] and by Mekmene *et al.* [3].

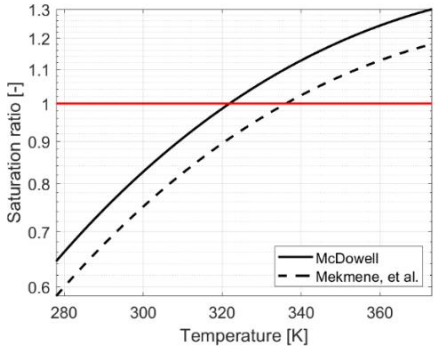

Fig. 2. Saturation ratio, calculated with equilibrium constant of McDowell *et al.* [10] (solid line) and by Mekmene *et al.* [3] (dashed line).

In this study the salting out of the solution due to the temperature increase is assumed to produce small primary particles, that can adhere on the heated surface. According to Mekmene *et al.* [4], in their experiments, the precipitates from the ultrafiltrated milk were aggregates formed of nanoparticles with a diameter of 100 nm. Therefore, the primary precipitates in here were assumed to be nanoparticles.

ISBN: 978-0-9984188-1-0; Published online www.heatexchanger-fouling.com

PARTICULATE FOULING

XDLVO theory applied to adhesion

The adhesion of the particles on the wall is affected by the electrical interaction between the colloidal particles and wall surface. The colloidal interactions of the van der Waals potential and the electrical double layer potential form the basis of DLVO theory of the colloid stability, developed by Derjaguin and Landau [12].

The London-van der Waals force arises from the interaction of fluctuating dipole moments, which are generated by the motion of electrons around the nuclei of neutral atoms in close vicinity of each other. The van der Waals interaction potential is attractive force, and for sphere–plate interacting geometries it is [13, 14]

$$f_{vdw} = -\frac{A_H r_p}{6a}, \qquad (6)$$

where A_H is the Hamaker constant, a is the distance between surfaces and r_p =50 nm is the radius of the particle. Hamaker constant is calculated based on the surface free energies [15]:

$$A_H = 0.24\pi H_0^2\left(\sqrt{g_1^{LW}} - \sqrt{g_3^{LW}}\right)\left(\sqrt{g_2^{LW}} - \sqrt{g_3^{LW}}\right) \qquad (7)$$

where particles (material index i=1) interact with a wall surface (i=2) while immersed in water (i=3). γ_i^{LW} is the Lifshitz–van der Waals component of the surface free energy of the material i and H_o = 0.158 nm is the minimum separation distance due to the Born repulsion.

While immersed in liquid, the solid bodies generally have an electrical surface charge, e.g., due to dissociation of surface groups. The surface charge makes the ions of opposite charge to be redistributed around the bodies. This phenomenon is responsible for the electronic double layer formation in the proximity of the body. For bodies of like sign, the force due to the double layer interactions is repulsive. The electrical double layer interaction is modeled as [16]

$$f_{edl} = \varepsilon_r\varepsilon_0\pi r_p\left[(z_1+z_2)^2\ln\left(1+e^{-\kappa a}\right) + (z_1-z_2)^2\ln\left(1-e^{-\kappa a}\right)\right] \qquad (8)$$

where ζ_1 and ζ_2 are the electrical surface potentials for the steel surface and the spherical particle at infinite separation and κ is the inverse of the Debye length. ε_r is the permittivity of the bulk calculated as temperature dependent [17]. The width of the electrical double layer (Debye length) is

$$\kappa^{-1} = \left(\frac{\varepsilon_r\varepsilon_0 RT}{2F_a^2 I\times 10^3}\right)^{1/2} \qquad (9)$$

where F_a is the Faraday constant, I the ion strength, R the gas constant and T the fluid temperature. Debye length is a measure of a charge carrier's net electrostatic effect in solution and describes how far its electrostatic effect persists.

The repulsion between the particles of like sign is influenced by added salt. The electrical surface potential decreases and the Debye length κ^{-1} decreases. Both these effects can decrease the repulsion force [13].

The attractive hydrophobic interactions can surpass the DLVO forces by two decimal orders of magnitude. The hydrophobic forces are due to the electron donor–electron acceptor interactions in polar media. For free energy due to the hydrophobic interaction, the model proposed by van Oss [15], modified for the sphere-plate case by Oliveira [16] was applied. The decay for the polar interaction between sphere and plate with distance a obeys:

$$f_{AB} = 2\pi l\, r_p \Delta G_{H_0}^{AB}\exp\left(\frac{H_0 - a}{l}\right) \qquad (10)$$

λ is the correlation length pertaining to water molecules, which is 0.6 nm for pure water. ΔG_{H0}^{AB} is the free energy of polar interactions at the distance of equilibrium. If material 1 interacts with material 2 while immersed in medium 3, the polar component of the free energy of the interaction is [15]

$$\Delta G_{H_0}^{AB} = 2\sqrt{g_3^+}\left(\sqrt{g_1^-}+\sqrt{g_2^-}-\sqrt{g_3^-}\right) + 2\sqrt{g_3^-}\left(\sqrt{g_1^+}+\sqrt{g_2^+}-\sqrt{g_3^+}\right) - 2\left(\sqrt{g_1^+ g_2^-}-\sqrt{g_1^- g_2^+}\right) \qquad (11)$$

Adhesion is determined by the balance between the attractive and repulsive forces. Hence, the total sum of the interaction potentials obtained from Eqs (6), (8) and (10) results in

$$f_T = f_{vdw} + f_{edl} + f_{AB}. \qquad (12)$$

In Fig. 3, the interaction potentials are presented. The potentials are calculated with the surface energies presented in Table 2. For electrical surface potential of steel, ζ_1 = -25 mV [18] and for HAP, ζ_2 = -5 mV [20, 21]. For particle diameter, 100 nm was applied [4].

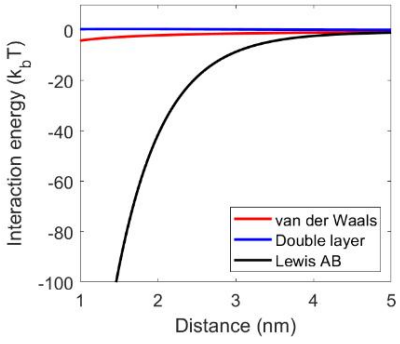

Fig. 3. Interaction potentials between HAP particle and steel surface according to XDLVO theory.

As seen in Fig. 3, the interaction potential due to the attractive hydrophobic interactions in SMUF

ISBN: 978-0-9984188-1-0; Published online www.heatexchanger-fouling.com

is significant in comparison to the interaction potentials due to the London-van der Waals force or the electrical double layer interaction. Therefore, it was noted that, e.g., the electrical surface potentials ζ_1 and ζ_2 did not have an effect on the resulting interaction potential.

Table 2. Surface energy parameters

	Water, [15] mJ/m^2	Stainless steel, AISI 316L [19] mJ/m^2	HAP [20] mJ/m^2
Non-polar component, γ^{LW}	21.8	42.8	28.5
Electron donor, γ^-	25.5	11.5	0.92
Electron acceptor, γ^+	25.5	2.0	16.0

CFD model for the particle fouling

In the CFD model for the particulate fouling, the electrical interaction energy between the surfaces of the particles and the wall determines the amount of deposited mass on the wall.

The methods of Spielman and Friedland [22] and Elimelech *et al.* [13] were used for incorporating the interaction energy into the calculation of particle flux at the wall. The rate of adhesion is calculated in this method from the electrical interaction potential barrier with the pseudo-first-order rate constant

$$K_f = D_B \left(\int_0^{d_D} \left(g_1(H) e^{f_T / k_b T} - 1 \right) dy \right)^{-1} \qquad (13)$$

where $g_1(H)$ is the hydrodynamic correction factor and H is the normalized distance between the surfaces. In order to ensure the total interaction energy f_{tot} equal to zero, the upper limit of the integration is thickness of the diffusion layer, δ_D ($>>\kappa^{-1}$). The interaction potential f_T is calculated as a total sum of the interaction potentials based on XDLVO (extended DLVO) theory, see Eq. (12).

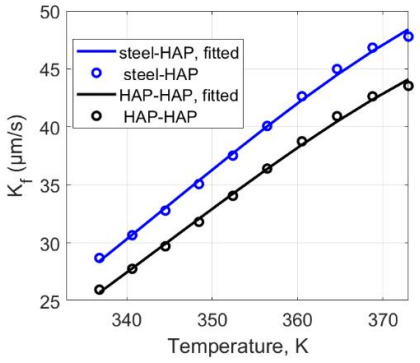

Fig. 4. Mass transfer coefficient K_f calculated for particle - clean steel surface and particle - fouled steel surface (presented with circles). Fitted curves as a function of temperature (solid lines).

In Fig. 4, the mass transfer coefficient K_f calculated from Eq. (13) is presented for the cases of particle - clean steel surface and particle - fouled steel surface at several temperatures (presented with circles). The fitted functions (solid lines) for the temperature dependency were applied in simulation.

The particle transport to the surface is calculated with a modified wall function approach based on convective-diffusion equation including the particle-wall interaction energy and the reduced mobility of the particle in the near-wall region presented earlier by Ojaniemi *et al.* [2]. Here, the approximate equation for solving the particle flux J_W to the wall from the bulk volume fraction α_b far away from the wall was obtained

$$\frac{J_W}{\alpha_b} = \left(\frac{r_p K_f v_{sg}}{v_{sg} e^B + K_f (e^B - 1)} \right) \qquad (14)$$

where B is a parameter depending on the turbulent viscosity obtained from the CFD simulation. For laminar fluid flow, the parameter B is dependent on the Brownian diffusion coefficient. v_{sg} is the slip velocity due to gravitation, and ρ_p is the density of the particles.

The simplified wall function model includes drag and diffusion, but thermophoresis, lift forces, and particle-particle interaction were neglected. Resuspension of the adhered particles was also neglected due to the low level of turbulence in the flow field in the experiments.

EXPERIMENTAL ARRANGEMENT

The results from the fouling test apparatus described by Jäsberg *et al.* [8] were used for the validation of the CFD model. The length of the flow channel is 140 mm, width is 40 mm and height (h_s) is 2 mm. Across a channel, there is a test section of a rectangular steel AISI 316L plate, which has a flow area of 32 × 40 mm^2 (see Fig. 5). The test plate is heated with a thermal conductor. Between the test plate and heater there is a solid metal block in contact with the plate.

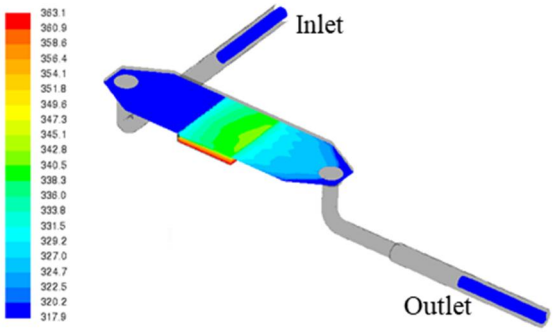

Fig. 5. CFD model of the test apparatus. Temperature (K) is shown on the bottom of the channel, and around the probes at inlet and outlet. The numerical grid consisted of 813 000 cells.

In the experiments, the apparatus was first heated to the experimental temperature with water, after which the SMUF solution was injected, see Table 1. The heating of the fluid was monitored by

ISBN: 978-0-9984188-1-0; Published online www.heatexchanger-fouling.com

the temperature difference measured with probes in the inlet and the outlet (see Fig. 5). Experiments were carried out at different heating powers, and with two mass flow rates.

3D SIMULATION RESULTS

Simulation method and boundary conditions

In the simulations, the material properties and boundary conditions were applied according to the experiments done by Jäsberg *et al.*[8]. The thermal dependencies of water density, viscosity, thermal conductivity and heat capacity were derived from the thermal data provided by NIST Chemistry Web book [23]. For the material density of HAP, the density of calcium phosphate 3140 kg/m^3 was applied.

The simulations were carried out with ANSYS Fluent code by applying the Algebraic Slip Mixture (ASM) model for the multiphase flow [24], including the species transport. For the interphase momentum exchange coefficient, the model of Schiller and Naumann provided by Fluent [24] was adequate due to the small size of the particles, which were assumed to be spherical.

For the modelling of turbulence with low Reynolds number, Shear-Stress Transport (SST) *k-w* Intermittency Transition model and LES model were applied [24]. SST *k-w* model is applicable to a wide class of wall bounded flows, and the Intermittency Transition model is recommended for the channel flows where no free stream is present.

In the LES model the large turbulent eddies are resolved numerically and only the small scale eddies having a slight effect on the large scale eddies are modelled with sub grid scale model (SGM).

The wall-bounded flows, as in the case of the experimental test channel, are demanding situations for LES modelling. The Wall-Adapting Local Eddy-Viscosity (WALE) model returns the correct near wall behaviour of turbulent viscosity ($\mu\, y^{+3}$) for wall bounded flows [24]. In addition, WALE returns a zero turbulent viscosity for laminar shear flows. From the models provided by ANSYS Fluent, the WALE model is then preferable model for the sub grid scale model in the studied case.

For heating the solid block under the test plate, the temperature boundary condition was applied at the bottom edge of the block. The evolving of the temperature inside the block was then simulated with CFD.

Simulation of water tests

CFD simulations of a test heat exchanger were first performed with water by using two mass flow rates, 300 mL/min and 600 mL/min. The Reynolds number $Re = \rho v h_s/\mu$ of the flow in the experimental channel was around 250 with the mass flow rate 300mL/min, and 500 with the mass flow rate 600 mL/min. Therefore, the flow was not fully turbulent and the model for turbulence had to be selected carefully. The numerical heat transfer model also had to be validated against plain water test before calculating tests performed with SMUF.

The steady state simulations were carried out by applying Shear-Stress Transport (SST) *k-w* Intermittency Transition model [24]. The unsteady simulations were carried out with LES model.

The calculated results for the mass weighted average temperature differences between inlet and outlet are compared to the experimental values in Fig. 6. The results are shown for the steady state simulations with Shear-Stress Transport (SST) *k-w* Intermittency Transition model [24]. The LES results were very close to SST *k-w* results, the difference was only 0.6%. The simulations with water were used in the calibration of the CFD model because in the experiments the contact between the solid metal block and the test plate caused additional thermal resistance R_θ=0.2K/W, evaluated with CFD.

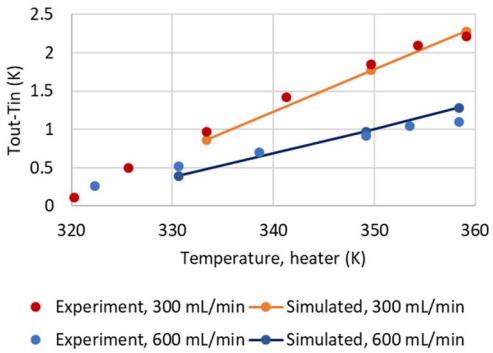

Fig. 6. Temperature difference between outlet and inlet. Experimental results are shown with dots. Calculated results are shown with lines and dots.

Simulation of fouling with SMUF

CFD model developed for the fouling of the heated surface was applied to experiments performed with SMUF. The unsteady simulation was carried out with LES.

In the CFD model the formation of the precipitates is described with mass source terms from the SMUF liquid phase to the particulate solid phase. The species concentrations exceeding the equilibrium concentrations are considered to form the solid phase, see Eq. (5). The precipitates form small (100 nm), spherical particles that can adhere on the wall surface according to the fouling model in Eq. (14).

The simulations were started with water, so that the temperatures were stabilized to the steady state corresponding to the experiments. Then, the concentrations according to SMUF recipe were added into the mass flow inlet and the species transport was calculated.

The fouling was assumed to start on the clean, smooth steel surface. Then, after the first particles were adhered on the surface, further particles were able to adhere on the top of the fouling layer. In

ISBN: 978-0-9984188-1-0; Published online www.heatexchanger-fouling.com

Fig.7 an example of the start of the simulation is presented with mass inflow rate of 300 mL/min. The coverage of the surface with foulants is gradually increasing and the flux on the top of the fouling layer is starting to take place. Coverage is calculated based on the number of the particles adhered on the surface assuming 63% packing density.

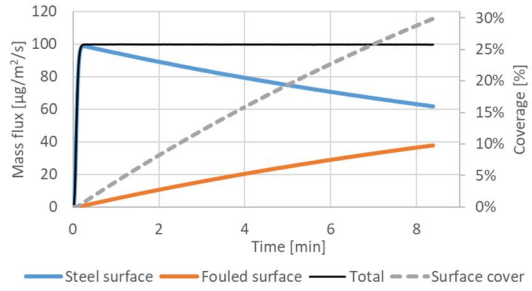

Fig. 7. Average mass flux on steel surface, on the fouled surface and the total average mass flux as a function of time. Coverage of the fouled surface is presented with dashed line (scale on the right).

The total mass flux of the foulants is the sum of the flux onto the clean surface and onto the fouled surface. The total average mass flux due to the fouling on the steel surface is levelling after the SMUF fluid with chemical components has passed the test plate.

The mass fluxes onto the clean, smooth steel surface and the already fouled surfaces has a small difference due to the different surface energies of the materials. As shown in Fig. 4., the mass transfer coefficient K_f onto steel surface is larger than onto the fouled surface.

In the simulations, the numerical model for the fouling predicted the saturation ratio exceeding one everywhere on the test plate, when the heater boundary condition was 363.15 K, and the saturation ratio was calculated with equilibrium constant of McDowell *et al.* [10]. Therefore, eventually the surface will be totally fouled, which is in agreement with the experimental results. It was also approximated from the calculated flux onto the fouled surface, that after 7,5 hours, the total amount of the fouled mass on the surface would be 3.4 mg with the flow rate of 300 mL/min, and 2 mg with the flow rate of 600 mL/min. In the experiments, the total precipitated mass with the flow rate of 300 mL/min was 20 mg. With the flow rate of 600 mL/min, the precipitated mass was 10 mg. Therefore, the predicted tendency of the fouling dependency on the flow was in agreement with the experiments.

In Figs. 8 to 12, CFD results from time instant of 8 minutes are presented, when the mass inflow rate is 300 mL/min and 600 mL/min. The direction of the flow is from left to right.

In Fig. 8, the temperature of the test plate surface is presented. Clearly, the temperature evolves higher with the lower mass inflow rate. This has an effect on the saturation ratio near the surface, and therefore on the fouling rate.

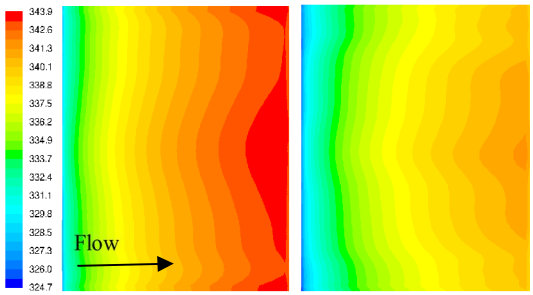

Fig. 8. Temperature (K) of the test plate. On the left: 300 mL/min, On the right: 600 mL/min.

In Fig. 9, the molar concentration of calcium (mol/L) is shown for the fluid flowing over the test plate. With the higher flow rate of 600 mL/min, the fluid was not heated as much as with the flow rate of 300 mL/min and the concentration of calcium did not decrease as much due to the precipitation. The initial concentrations shown in Table 1 were applied in the simulations.

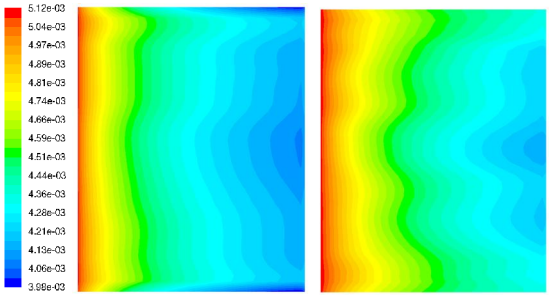

Fig. 9. Molar concentration of calcium ion (mol/L). On the left: 300 mL/min, On the right: 600 mL/min.

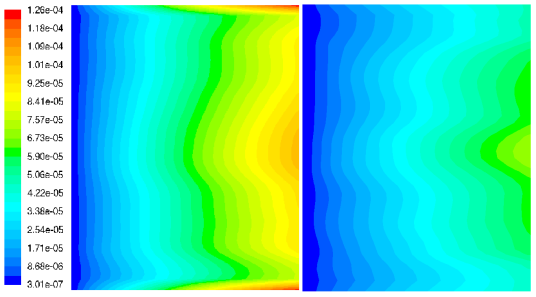

Fig. 10. Particle volume fraction (-). On the left: 300 mL/min, On the right: 600 mL/min.

In Fig.10, the particle volume fraction in the near-wall region of the test plate surface is presented. The amount of the particles is larger, when mass flow rate is smaller. This is in agreement with the decrease of the molar concentration of calcium, which is presented in Fig. 9. The particles formed at the inflow edge of the test plate, which are not immediately deposited on the wall, are transported over the plate with fluid flow, and possibly adhered later on the surface. The

ISBN: 978-0-9984188-1-0; Published online www.heatexchanger-fouling.com

distribution of foulant mass flux on the test plate surface is presented in Fig.11. The surface coverage distribution is proportional to the mass flux of the foulants, see Fig.12. The fouling of the test plate is proceeding from the outer edge, which is in agreement with the experiments [8].

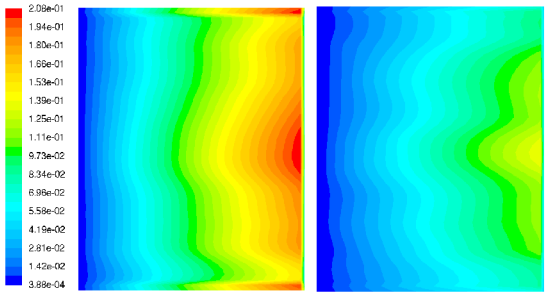

Fig. 11. Mass flux on the surface (mg/m^2/s). On the left: 300 mL/min, On the right: 600 mL/min.

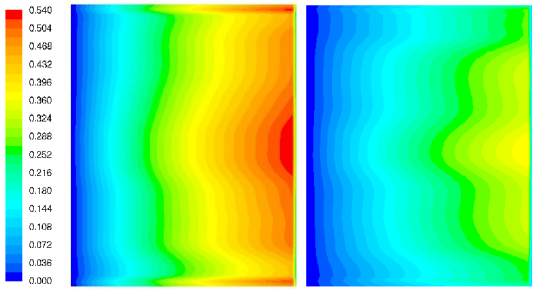

Fig. 12. Surface coverage (-). On the left: 300 mL/min, On the right: 600 mL/min.

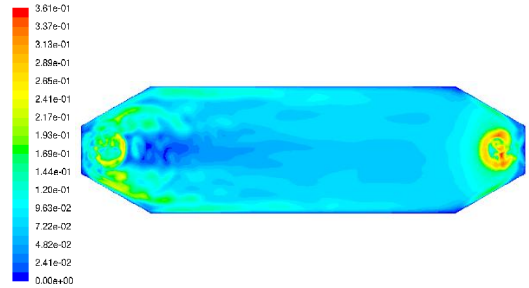

Fig. 13. Velocity magnitude (m/s) near the bottom surface of the apparatus. Mass flow rate 600 mL/min.

The results shown in Figs. 8 to 12, are instantaneous results obtained with LES model. The flow inside the channel is fluctuating, and therefore time dependent. In Fig. 13 the instantaneous velocity magnitude is presented over the bottom surface in the test apparatus when the mass inflow rate is 600 mL/min.

As shown in Fig. 13, the flow field is fluctuating even above the test plate. In the region of the test plate the maximum flow velocities occur near the side walls of the channel. The effect of the flow field is seen in the time instantaneous distributions and in the time-averaged distributions close to the side walls.

CONCLUSION

A CFD model was developed for fouling of calcium phosphate in heat exchangers that can take into account the tendency of fluid components to precipitate and the surface properties of the materials. The model was tested against experiments made with SMUF. The tendency of the fouling distribution and the magnitude of the results for fouled masses were in rough agreement with the experiments. In the model, mechanical entrapment due to the surface roughness or precipitated particles is not taken into account, neither agglomeration of the particles, or growth of the precipitated particles at the surface. The present model is not taking into account the effect of the fouled layer on the heat transfer. However, this is not significant while using the model in predicting the fouling distribution onto a clean surface.

The model has the potential in applying it in the predicting of the milk deposition profile in heat exchangers. The potential usage is in designing the plate shape, corrugation profile and surface materials in order to reduce fouling. The significance of the developed model is that there is no need for fitting the model parameters. The applied parameters are taken from the experiments or from literature.

NOMENCLATURE

a distance between surfaces, m
$a(X^{Y+})$ activity of ion X^{Y+}
A_H Hamaker constant, J
c_i molar concentration of specie i, mol/L
d_p particle diameter, m
D diffusion coefficient, m^2/s
ΔH^0 standard reaction entalphy, kJ/mol
H_o minimum separation distance, 0.158 nm
h_s height of the channel, m
I ion strength, mol/L
J_W flux, kg/(m^{2}s)
k_b Boltzmann constant, $1.3807 \cdot 10^{-23}$ J/K
K_f mass transfer rate, m/s
K_T equilibrium constant at temperature T
R universal gas constant, 8.3144 J/(K·mol)
T temperature, K
v velocity across the channel, m/s
v_{sg} slip velocity due to gravitation, m/s
y distance from surface, m
α volume fraction, dimensionless
ε_0 permittivity of vacuum, $8.854 \cdot 10^{-12}$ C^2/(m·J)
ε_r relative permittivity
ζ electrical surface potential, mV
λ thermal conductivity, W/(m·K)
correlation length, 0.6 nm
μ viscosity, kg/(m·s)
ρ density, kg/m^3
f interaction energy between surfaces, J
z_i charge number of ion i
γ activity coefficient, surface energy

ISBN: 978-0-9984188-1-0; Published online www.heatexchanger-fouling.com

Subscript

i index
b bulk
p particle
AB Lewis acid-base
LW Lifshitz-van der Waals
edl electrical double layer
vdw London-van der Waals

ACKNOWLEDGEMENT

The research leading to these results has received funding from Academy of Finland under grant agreement no. 298404.

REFERENCES

[1] Sadeghinezhad, E., Kazi, A. B., Badarudin, A., Zubair, M. N. M., Dehkordi, B. L. D., and Oon, C. S., A review of milk fouling on heat exchanger surfaces, *Rev. Chem. Eng*., Vol. 29, pp. 169–188, 2013.

[2] Ojaniemi, U., Riihimäki, M., Manninen, M., Pättikangas, T., Wall function model for particulate fouling applying XDLVO theory, *Chem. Eng. Sci*., 84, pp. 57-69, 2012.

[3] Mekmene, O., Quillard, S., Rouillon, T., Bouler, J.-M., Piot, M., Gaucheron, F., Effects of pH and Ca/P molar ratio on the quantity and crystalline structure of calcium phosphates obtained from aqueous solutions, *Dairy Sci. Technol*. 89, pp. 301–316, 2009.

[4] Mekmene, O., Leconte, N., Rouillon, T., Quillard, S., Bouler, M., Gaucheron, F., Physicochemical characterisation of calcium phosphates prepared from milk ultrafiltrates: Effect of the mineral composition, *Int. J. Dairy Technology*, Vol 65, No 3, 2012.

[5] Rice, G., Barber, A., O'Connor, A., Stevens, G., Kentish S., A theoretical and experimental analysis of calcium speciation and precipitation in dairy ultrafiltration permeate, *Int. Dairy Journal*, 20, pp. 694-706, 2010.

[6] Castro, F., Ferreira, A., Rocha, F., Vicente, A., Teixeira, J.A., Characterization of intermediate stages in the precipitation of hydroxyapatite at 37 ºC, *Chem. Eng. Sci*. 77, pp. 150–156, 2012.

[7] Dumpler, J., Kieferle, I., Wohlschl€ager, H., Kulozik, U., Milk ultrafiltrate analysis by ion chromatography and calcium activity for SMUF preparation for different scientific purposes and prediction of its supersaturation, *Int. Dairy Journal*, 68, pp. 60-69, 2017.

[8] Jäsberg, A., Turpeinen, T., Ketola, A., Ojaniemi, U., Pättikangas, T., Koponen, A., Fouling dynamics of SMUF on a plate heat exchanger, submitted to Heat Exchanger Fouling and Cleaning – 2019, June 2–7, 2019, Warsaw, Poland.

[9] Schmidt, D. G., Both, P., Studies on the precipitation of calcium phosphate. I. Experiments in the pH range 5.3 to 6.8 at 25 ºC and 50 ºC in the absence on additives, *Netherlands Milk and Dairy Journal*, 41, pp. 105-120, 1987.

[10] Mc Dowell H., Gregory T.M., Brown W.E., Solubility of $Ca_5(PO_4)_3OH$ in the system $Ca(OH)_2$-H_3PO_4-H_2O at 5, 15, 25, and 37 °C, *J. Res. Nat. Bur. Stand*., 81, pp. 273–281, 1977.

[11] La Iglesia, A., Estudios Geol., 65(2), pp. 109-119, julio-diciembre. ISSN: 0367-0449, 2009.

[12] Derjaguin, B.V., Landau, L.D., *Acta Physicochim* Vol. 14, pp. 733., 1941.

[13] Elimelech, M., Greory, J., Jia, X., Williams, R.A., Particle Deposition and Aggregation - Measurement, Modelling and Simulation, Elsevier, 1995.

[14] Epstein, N., Elements of Particle Deposition onto Porous Solid Surfaces Parallel to Suspension Flows, *Experimental Thermal and Fluid Science* 14, pp. 323-334, 1997.

[15] Van Oss, C.J., Interfacial forces in Aqueous media, 2nd ed., Marcel Dekker, New York, 2006.

[16] Oliveira, R., Understanding Adhesion: A Means for preventing fouling, *Experimental Thermal and Fluid Science*, 14, pp. 316-322, 1997.

[17] Handbook of Chemistry and Physics, 1998. CRC Press, Boca, Raton.

[18] Boulangé-Petermann, L., Doren, A., Baroux, B., Bellon-Fontaine, M-N., Zeta potential measurements on passive metals, *J. Colloid Interface Sci.* 171, pp. 179-186, 1995.

[19] Santos, O., Nylander, T., Roshmaninho, R., Rizzo, G., Yiantsios, S., Andritsos, N., Karabelas, A., Müller-Steinhagen, H., Melo, L., Boulangé-Petermann, L., Gabet, C., Braem, A., Trägårdh, C., Paulsson, M., Modified stainless steel surfaces tar-geted to reduce fouling – surface characterization", *J. Food Eng*., 64, pp. 63-79, 2004.

[20] Liu, Y., Nancollas, G.H., Crystallization and Colloidal Stability of Calcium Phosphate Phases, *J. Phys. Chem. B*, 101, pp. 3464-3468, 1997.

[21] Anema, S. G., Stability of milk-derived calcium phosphate suspensions, *Dairy Sci. Technol*. 89, pp. 269–282, 2009.

[22] Spielman, L.A., Friedlander, S.K., Role of electrical double layer in particle deposition by convective diffusion, *J. Colloid Interface Sci.* Vol. 46, pp. 22-31, 1973.

[23] NIST Chemisty Web Book: http://webbook.nist.gov/chemistry/

[24] Fluent, Ansys Fluent Theory guide – Release 16.0, Ansys Inc, 2015.

ISBN: 978-0-9984188-1-0; Published online www.heatexchanger-fouling.com